N-cadherin facilitates trigeminal sensory neuron outgrowth and target tissue innervation

Caroline Halmi[1], Alec McIntosh[2], Carrie E. Leonard[1], Lisa A. Taneyhill[1,*]

[1]Department of Animal and Avian Sciences, University of Maryland, College Park, MD 20742 USA

[2]Lombardi Comprehensive Cancer Center, Georgetown University, Washington, DC, 20007 USA

Email: ltaney@umd.edu

*Corresponding author

ABSTRACT

During the development of the sensory nervous system, various cell types converge to form different tissues. The trigeminal ganglion houses the cell bodies for the trigeminal nerve and exemplifies these intercellular interactions, as it is formed from the condensation of two diverse precursor cell populations, neural crest cells and placode cells. The dual origin of the trigeminal ganglion has been understood for decades, but the molecules that orchestrate this process remain relatively unknown. Assembling the trigeminal ganglion is mediated by cell adhesion molecules including the protein neural cadherin (N-cadherin), expressed first in placode-derived neurons and later in all trigeminal sensory neurons. Prior studies have shown that N-cadherin knockdown in chick trigeminal placode cells leads to early defects in trigeminal ganglion assembly by impacting the ability of placode-derived neurons to properly condense with undifferentiated neural crest cells. Later functions for N-cadherin in chick trigeminal gangliogenesis, however, are unknown. Using morpholino-mediated knockdown of N-cadherin in chick trigeminal placode cells, we examined trigeminal ganglion development at later developmental stages, when neural crest cells are differentiating into neurons. Through these experiments, we uncovered a sustained negative impact on the trigeminal ganglion, leading to decreases in ganglion size, nerve outgrowth, and branching to target tissues *in vivo*. Further, blocking the adhesive function of N-cadherin reveals its importance in the outgrowth ability for some, but not all, trigeminal neurons *in vitro*. These deficits reflect potential cell and non-cell autonomous effects on placodal and neural crest-derived neurons, respectively, and point to the importance of N-cadherin-mediated adhesion among trigeminal sensory neurons. Our findings reveal continued adhesion-dependent functions for N-cadherin in the trigeminal ganglion, which will aid in the understanding of its tissue-specific roles.

INTRODUCTION

The development of an advanced nervous system has contributed, in part, to the evolution of more complex organisms like vertebrates that can sense their surroundings and respond to environmental cues. To this end, neurons of the peripheral nervous system transmit sensory information from the body back to the brain. A portion of these neurons condense into sensory ganglia, and specifically within the head, are known as cranial ganglia. While some of the cranial nerves function to transmit only sensory information or motor information, a subset of them conveys both. Of the five cranial nerves (trigeminal, facial, glossopharyngeal, vagus, and spinal accessory), the paired trigeminal nerves are unique in that they are the largest of all the cranial nerves and extensively innervate many facial regions. The trigeminal nerve is comprised of three major branches - the ophthalmic, maxillary, and mandibular - that innervate the forehead and eye region, upper jaw, and lower jaw, respectively. While all three branches relay sensory information, only the mandibular branch has motor neurons that aid in mastication.

The chick embryo has proved to be an exemplary model in understanding many developmental processes, including discerning the cell types that comprise the trigeminal ganglion[1,2]. Both neural crest cells and neurogenic placode cells contribute neurons to the trigeminal ganglion[1], while the neural crest also form glial cells. These embryonic cell populations are derived from the ectoderm and arise at the neural plate border, located between the non-neural ectoderm and the neural plate[3]. During early neural development, neural crest cells reside in the future neural folds, where they subsequently undergo an epithelial-to-mesenchymal transition to delaminate from the dorsal neural folds and become motile. Neural crest cells that contribute to the trigeminal ganglion originate from the midbrain and anterior hindbrain[4,5]; however, the neural crest as a cell population are found throughout the body axis and are capable of differentiating into numerous different cell types including cranial bone and cartilage, melanocytes, chromaffin cells, cardiac myocytes, and neurons of the peripheral nervous system[6]. Cranial neural crest cells collectively migrate through the embryonic head using a combination of chemoattraction and repulsion and mechanical sensing[7,8]. Trunk neural crest cells differ from the cranial neural crest in a number of ways including their derivatives, multipotent abilities, and migratory methods[7].

Cranial neurogenic placodes are specialized regions of thickened ectoderm that differentiate into neurons prior to ingression[9]. Initially, there is slight overlap between the different placodes that comprise the cranial ganglia; however, as development progresses, the placodes become more segregated and distinct[10]. The trigeminal placode, which consists of the ophthalmic and maxillomandibular placodes, gives rise to all the placode-derived neurons of the trigeminal ganglion. Although these two placodes work together to produce one structure, the placodes differ from one another in two important ways. First, the ophthalmic and maxillomandibular placodes contribute neurons to distinct lobes of the trigeminal ganglion (ophthalmic, and maxillary and mandibular, respectively). Second, the majority of the cells to which the ophthalmic placode gives rise are post-mitotic, traveling to the trigeminal ganglion as differentiated neurons, while the maxillomandibular placode generates neuroblasts that do not differentiate until they have reached the trigeminal ganglion[11–14]. Notably, in the chick, placodal neurons are the first neurons present within the trigeminal ganglion, and are located distally compared to neural crest-derived neurons, which are more proximal and form later during development[2,15].

Prior studies have led to great advancements in understanding the complex interactions that occur between neural crest and placodal neurons during their early migration and the subsequent onset of gangliogenesis. Like neural crest cells, placodal neurons are also capable of collective migration[16,17]. While the molecular mechanisms behind these movements are poorly understood, the cellular basis of this involves neural crest cells forming corridors to facilitate this process[18], as they are a more permissive substrate compared to the surrounding mesoderm. Furthermore, neural crest and placode cells exhibit “chase and run” behavior, where neural crest cells promote the migration of placode cells to their terminal destinations[16]. These two reports, in addition to other studies, indicate an intricate dynamic between these two cell types that point to important reciprocal interactions[1,19,20]. Although much has been understood about the influence of neural crest cells on surrounding cell types, placode cells included, there is still limited knowledge about how placodal neurons influence the migration and differentiation of neural crest cells.

The earliest populations of neurons within a system are known as pioneer neurons, as they migrate to targets first and provide a scaffold for later born neurons to grow along[21]. While there is some understanding of the function of pioneer neurons within vertebrates[22–24], much of our knowledge in this area has come from studies in invertebrates[25–28]. Still, there is conflicting data about whether pioneer neurons are necessary and unique cells, and additionally, their importance appears to be system-dependent. Within the trigeminal ganglion, there is very limited information surrounding the function and relevance of pioneer neurons. One study in mouse found the earliest trigeminal neurons of the ophthalmic lobe reaching their targets by embryonic day (E) 9.5[29]. Within the chick, the use of a monoclonal antibody against beta-tubulin III (Tubb3) has aided in understanding that placode cells express Tubb3 before they leave the ectoderm, while neural crest cells express Tubb3 later, after they differentiate into neurons[30]. This is in keeping with findings on the timeline of trigeminal sensory neuron differentiation in the chick – placode- and neural crest-derived neurons become post-mitotic and differentiate within 2-5 days and 4-7 days of incubation, respectively[15]. During this time, the placodal neurons are beginning to grow towards the periphery and are making their initial connections with their targets. This cumulative knowledge suggests that placodal neurons are pioneers that serve as templates for the later differentiating neural crest-derived neurons to grow and extend axons[30]; however, this has never been definitively proved. Furthermore, molecules orchestrating this process remain unknown.

The migratory abilities of neural crest and placode cells, as well as the interactions between the two to form the trigeminal ganglion[31], are mediated by cell-cell adhesion. More specifically, cadherins, which are transmembrane proteins that function in strengthening adhesion between adjacent cells, have been shown to play an important role in gangliogenesis. The extracellular domain of a cadherin can participate in *cis* or *trans* interactions. Although cadherins generally engage in homophilic interactions, they are capable of interacting heterophilically as well[32–34]. The cadherin intracellular domain contains two binding sites for catenin proteins. The interaction between a cadherin and p120-catenin regulates the availability of the cadherin at the membrane and its ability to engage in adhesion, while cadherin binding to β-catenin and α-catenin serves to link the cadherin to the actin cytoskeleton[35].

The cadherin profile of a cell is dynamic and can change depending on the needs of the cell. Premigratory cranial neural crest cells initially express Cadherin-6B prior to their delamination and subsequent epithelial-to-mesenchymal transition, but once migratory, begin expressing Cadherin-7[36], a type-II cadherin which aids in transient cell-cell adhesion. In the chick, the first expression of neural cadherin (N-cadherin) is seen as early as 24 hours into development and is localized to the neural plate. N-cadherin expression persists as the neural plate grows and becomes the neural tube[37]. Further, placode cells and their neuronal derivatives express N-cadherin prior to delaminating from the ectoderm[38]. This is not surprising given that prior studies have shown that N-cadherin possesses important roles during neurodevelopment including regulating neurite outgrowth[39], axonal fasciculation[40], and proper synapse formation[41,42]. All of the listed examples highlight adhesion-dependent roles of N-cadherin during neurodevelopment; however, N-cadherin can also play adhesion-independent roles such as controlling neural differentiation and acting as a modulator of various signaling pathways[43,44].

While N-cadherin expression in trigeminal placode cells is critical for initial stages of gangliogenesis and the ability for early trigeminal neurons to condense[38], whether there is a need for N-cadherin throughout the development of the trigeminal ganglion and its nerves remains unknown. Furthermore, how the early expression of N-cadherin within placodal neurons impacts all the neurons of the trigeminal ganglion is not understood. Here, we show that placodal expression of N-cadherin is important throughout gangliogenesis, with defects to morphology observed in both the ganglion as well as projections to target tissues upon N-cadherin depletion from placode cells. Additionally, we show a reduction to axonal projections both *in vivo* and *in vitro* that can be attributed to a loss of N-cadherin-mediated adhesion. These results suggest that trigeminal neurons depend on the adhesive function of N-cadherin, initially expressed in placodal neurons, to facilitate their outgrowth.

170 **MATERIALS AND METHODS**

171 **Chick embryos**

172 Fertilized chicken eggs (*Gallus gallus*) were obtained from the Department of
173 Animal and Avian Sciences at the University of Maryland and Centurion Poultry
174 Incorporated (GA) and incubated at 37 °C in humidified incubators on their sides.
175 Embryos were incubated to reach desired Hamburger Hamilton (HH) stages based on
176 times provided therein[45]. Embryos were staged with this method or by counting the
177 number of somite pairs (somite stage, ss).

178

179 **Morpholinos**

180 To reduce N-cadherin protein expression, a validated lissamine-tagged translation-
181 blocking morpholino antisense oligonucleotide (MO) against N-cadherin was used
182 (GeneTools, LLC)[38], with a sequence of 5'-GCGGCGTTCCCGCTATCCGGCACAT-3'. For
183 control experiments, a 5 base pair mismatch N-cadherin control MO was used[38], with a
184 sequence of 5'-GCGcCcTTCCCcCTATgCcGCACAT-3' (altered base pairs in lowercase).
185 Both MOs were used at a final concentration of 500 μM and were diluted with ultrapure
186 water and 10% sucrose (in 1X phosphate-buffered saline (PBS)).

187

188 ***In ovo* unilateral placode electroporation**

189 To target trigeminal placode cells prior to their delamination, a unilateral
190 electroporation was performed at HH10-11. Briefly, the N-cadherin MO or N-cadherin
191 mismatch MO (MM) was expelled on top of the ectoderm on one side of the embryo using
192 a fine glass needle. Next, a 30-gauge needle was used to puncture a small hole through
193 the vitelline membrane so that electrodes could lay vertically above and below the
194 ectoderm over which the MO had been placed. Three, 9V pulses were delivered over 50
195 ms at 200 ms intervals. After electroporations, eggs were resealed with tape and parafilm
196 and grown at 37 °C to desired stages of interest. Due to the inherent variations that arise
197 during normal development, even when embryos are staged identically, the contralateral
198 side of the electroporated embryo was a more appropriate control and was used for all *in*
199 *vivo* studies. Initial experiments comparing N-cadherin MO-electroporated embryos to N-
200 cadherin control MO-electroporated embryos were done to ensure none of the reported

201 phenotypes was due to the electroporation method. All embryos were screened for
202 successful MO electroporation based on the red fluorescence of the MO prior to collection
203 and use in subsequent assays.
204
205 **Immunostaining**
206 Electroporated embryos were grown to desired stages of interest, collected, and
207 fixed in 4% paraformaldehyde (PFA) overnight at 4°C with agitation. Following fixation,
208 embryos were washed 3 x 10 minutes in 1X PBS and stored in 1X PBS at 4°C until further
209 processing. Primary antibodies used included Tubb3 (Abcam, 1:500 for section, 1:250 for
210 whole-mount) and Sox10 (GeneTex, 1:250). Secondary antibodies used included
211 goat@rabbit 405 (ThermoFisher) and goat@mouse IgG_{2a} 555 or 647 (SouthernBiotech).
212 **Tissue sections:** Embryos were processed through an increasing sucrose
213 gradient (5% and 15% sucrose (Fisher) in 1X PBS) either overnight at 4°C or until they
214 sank to the bottom of the vials. Next, they were processed through 7.5% gelatin (Sigma)
215 in 15% sucrose and 20% gelatin in 1X PBS, both at 37°C, either overnight or until the
216 tissue sank. Embryos were embedded in 20% gelatin, flash-frozen using liquid nitrogen,
217 and stored at -80°C until ready for use. Embedded embryos were then cryo-sectioned at
218 12μm on charged slides (VWR). Slides were stored at -20°C until ready for use. For
219 immunohistochemistry, slides were de-gelatinized by incubation in 1X PBS at 42°C for
220 15-20 minutes. Following 3 x 5-minute washes in 1X PBS, the slides were blocked with
221 10% heat-treated sheep serum (HTSS) in PBST (Sigma, 1X PBS + 0.1% Triton) at room
222 temperature for 1-2 hours in a humidified chamber, then rinsed in PBST (0.1%). Primary
223 antibodies were diluted in PBST + 5% HTSS, added to the slides, covered with a glass
224 coverslip (Fisher) to prevent sections from drying out, and incubated overnight at 4°C.
225 The following day, the coverslips were removed, and the slides were washed 4 x 30
226 minutes in PBST. Secondary antibodies were then diluted in PBST + 5% HTSS, added to
227 the slides, covered with a glass coverslip, and incubated overnight at 4°C. The next day,
228 slides were again washed 4 x 30 minutes in PBST and mounted with DAPI-fluoromount
229 media (SouthernBiotech).
230 **Standard whole-mount:** Embryos were blocked with 10% HTSS in PBST (0.1%)
231 for 2 hours at room temperature. Following a rinse with PBST, primary antibodies were

232 diluted in PBST + 5% HTSS and incubated overnight at 4°C with agitation. The following
233 day, the embryos were washed 4 x 30 minutes in PBST. Secondary antibodies were
234 diluted in PBTS + 5% HTSS and incubated overnight at 4°C with agitation. The next day,
235 embryos were again washed 4 x 30 minutes in PBST and stored in 1X PBS at 4°C until
236 they were either imaged or FRUIT cleared.

237 **Modified whole-mount for iDISCO clearing:** Fixed embryos were washed 2
238 times for 1 hour in 1X PBS and then were taken through an increasing methanol (MeOH
239 in 1X PBS) gradient (50% (1 x 1 hour), 80% (1 x 1 hour), 100% (2 x 1 hour)), before they
240 were bleached overnight in 5% H_2O_2 in 20% DMSO (Fisher)/methanol at 4°C. The next
241 day, samples were taken through the following series of washes: 2 x 1 hour in 100%
242 MeOH, 2 x 1 hour in 20% DMSO/MeOH, 1 x 1 hour in 80% MeOH, 1 x 1 hour in 50%
243 MeOH, 2 x 1 hour in 1X PBS, and 2 x 1 hour in PBST (0.2%). Samples were incubated
244 overnight in 20% DMSO/0.3M glycine (Fisher)/PBST at 4°C. The next day, samples were
245 blocked in 10% HTSS/10% DMSO/PBST overnight at 4°C. Embryos were washed 2 x 1
246 hour in 0.2% Tween-20 (Sigma)/1X PBS with 10 µg/mL heparin (Fisher, PTwH) at room
247 temperature before primary antibodies were added and incubated for 72 hours at 4°C.
248 Primary antibodies were diluted in 5% DMSO/5% HTSS/PTwH. Samples were washed in
249 PTwH for 24 hours before secondary antibodies were added (diluted in the same manner
250 as the primary antibodies), and samples were incubated with secondary antibodies for 48
251 hours at 4°C. Samples were then washed for 48 hours in PTwH before iDISCO clearing.

252 **Explant immunocytochemistry:** Explant slides were washed once with 1X PBS,
253 followed by fixation in 4% PFA for 1 hour at room temperature with agitation. Following
254 fixation, slides were rinsed with 1X PBS and stored in 1X PBS at 4°C until ready for
255 immunocytochemistry. A hydrophobic perimeter was drawn around the slides to prevent
256 dehydration of tissue using an ImmEdge Pen (Vector Laboratories), and explants were
257 taken through blocking, primary antibody incubation, and secondary antibody incubation
258 in the absence of coverslips as described in the tissue section methods. Slides were
259 mounted with DAPI-fluoromount media (SouthernBiotech) and covered with a glass
260 coverslip.
261
262

263 **Tissue clearing**

264 As embryos progress through development and tissue structures surrounding the
265 trigeminal ganglion become more complex, visualization of the trigeminal ganglion after
266 whole-mount immunohistochemistry became increasingly difficult. Therefore, clearing
267 methods to render the tissues transparent were performed. At early stages (up to HH22),
268 the FRUIT[46] tissue clearing protocol was used, whereas later stages required iDISCO[47]
269 tissue clearing. With both protocols, MO signal was quenched during the clearing
270 processes.

271 **FRUIT:** Following the standard whole-mount immunohistochemistry protocol,
272 embryos were progressed through increasing concentrations of a fructose/urea cocktail
273 (35%, 40%, 60% and 80%) for a minimum of 8 hours, up to 24 hours at room temperature,
274 depending on the stage of the embryo. The time spent in a certain concentration of FRUIT
275 buffer was determined based on how quickly the sample was rendered transparent. A
276 sample was only moved up to the next FRUIT buffer once it had visibly changed
277 transparency. The cocktail, containing 8M urea (Sigma), 0.5% (v/v) alpha-thioglycerol
278 (Fisher), and increasing concentrations of fructose (Sigma), was made by first dissolving
279 the fructose in ultrapure water at 37 °C. Once dissolved, the urea was added, and the
280 solution was rocked at room temperature until homogenous. Lastly, alpha-thioglycerol
281 was added, and the buffers were stored at 4°C until use. Following clearing, embryos
282 were imaged in 60% or 80% (depending on the stage of the embryo) FRUIT buffer in
283 glass-bottomed petri dishes. Typically, embryos up to HH19 were imaged in 60% FRUIT
284 while HH20-22 staged embryos were imaged in 80% FRUIT.

285 **iDISCO:** Following the modified whole-mount immunohistochemistry protocol,
286 embryos were washed in PBST (0.2%) for a minimum of 48 hours. Samples were
287 incubated in 50% (v/v) tetrahydrofuran (THF, Sigma)/water overnight at room temperature
288 in glass vials, making sure that over 90% of the vial was filled with the solution. The
289 following day, embryos were then incubated in 80% THF/water for one hour at room
290 temperature, followed by 2 x 1-hour incubations in 100% THF. Next, samples were
291 incubated in 100% dichloromethane (Sigma) for 1-2 hours (or until they sank to the bottom
292 of the vial). Lastly, embryos were incubated in dibenzyl ether (DBE, Sigma) overnight and
293 imaged the following day in DBE. Embryos were stored in DBE at room temperature.

294 iDISCO-cleared embryos were imaged in a glass petri dish containing a 3D chamber[47],
295 which was printed in Terrapin Works, part of the School of Engineering at the University
296 of Maryland.
297
298 **TUNEL assay**
299 To assess apoptosis, the *In Situ* Cell Death Detection Kit, Fluorescein (Roche) was
300 used according to manufacturer's instructions. Briefly, following secondary antibody
301 washes (4 x 30 minutes in PBST (0.1%)), slides were washed once for 30 minutes in 1X
302 PBS. Slides were re-fixed with 4% PFA for 20 minutes at room temperature, followed by
303 one 30-minute wash in 1X PBS. The TUNEL reaction mixture was added to the slides (75
304 µL per slide), and a glass coverslip was placed over them. Slides were incubated in the
305 dark for 1 hour at 37°C. Next, the coverslips were removed, and the slides were washed
306 3 x 5 minutes in 1X PBS. Lastly, slides were mounted with DAPI-fluoromount media
307 (SouthernBiotech).
308
309 **Trigeminal ganglion explant assay**
310 Wild-type HH13/14 embryos were dissected from eggs and stored on ice in 1X
311 PBS until dissections. Trigeminal ganglia were dissected on a sylgard-coated dish by first
312 bisecting the embryo and then carefully taking the area of the forming trigeminal ganglion,
313 making sure to exclude the eye and neural tube. Explants were cultured on 2-well glass
314 chamber slides (ThermoFisher) coated with Poly-L-lysine (0.01% PLL, Sigma) and
315 fibronectin (0.01%, Sigma). To make the coated slides, 1 mL of PLL (diluted in ultrapure
316 water) was added to each chamber on the glass slides and incubated inside a biosafety
317 cabinet for 30 minutes at room temperature. The PLL was removed, and slides were
318 washed 3 times with water. Next, 1 mL of fibronectin (diluted in DMEM media
319 (ThermoFisher)) was added to each chamber and incubated at 37°C for a minimum of 2
320 hours. The fibronectin solution was removed, and slides were stored at 4°C until needed.
321 Explants were grown in DMEM media supplemented with N2 (1:100, ThermoFisher) and
322 Penicillin/Streptomycin (1:100, Fisher).
323
324

325 **N-cadherin function-blocking antibody experiments**

326 After 24 hours of incubation, fresh media containing either the MNCD2 function
327 blocking antibody (DSHB, 0.1μg/mL), or a normal rat IgG control (Santa Cruz
328 Biotechnology, 1.6 μg/mL), was added to the explants to replace the current media, and
329 explants were incubated overnight. The following morning, the slides were briefly rinsed
330 with 1X PBS, and then fixed in 4% PFA for one hour at room temperature. The explants
331 were washed 3 times in 1X PBS, and then processed for immunocytochemistry.

332

333 **Confocal imaging**

334 All images were acquired with the LSM Zeiss 800 confocal microscope with
335 Airyscan detection (Carl Zeiss Microscopy, Thornwood, NY, USA). Laser power, gain, and
336 offset were kept consistent for the different channels during all experiments where
337 possible. ImageJ (NIH)[48,49] and Adobe Photoshop CC 2023 were used for image
338 processing. For whole-mount imaging with Z-stacks, all embryos were imaged at a 5μm
339 interval. For sections, images of at least five serial transverse sections were acquired and
340 used for analysis. For all experiments, a minimum of five replicates were obtained.

341

342 **Quantifications and statistical analyses**

343 **Surface area:** For modified surface area measurements of the whole trigeminal
344 ganglion, the OpV lobe, and the MmV lobes, maximum intensity Z-projections were first
345 generated from Z-stacks taken through the trigeminal ganglion using ImageJ. The
346 polygon tool was used to outline the perimeter of Tubb3 signal and area measurements
347 were generated. Individual area measurements for each developmental stage grouping
348 were averaged together and plotted to generate graphs.

349 **Sox10 and TUNEL cell counting:** N-cadherin MO-treated embryos were
350 processed for section immunohistochemistry for Sox10 and Tubb3, followed by the
351 TUNEL staining protocol. Once imaged, the individual channels were opened on ImageJ.
352 With the Tubb3 channel image, the polygon tool was used to trace the outline of the
353 trigeminal ganglion. The outline was added to Region of Interest (ROI) manager, and then
354 used to crop both the TUNEL channel and Sox10 channel to only include the area of the
355 image that contained neurons of the trigeminal ganglion. Once images from all

experiments were processed, they were analyzed using the Squassh[50] plugin from the MOSAICsuite in ImageJ, as described[34]. Segmentation parameters were kept uniform for all images in one experimental condition (Sox10 or TUNEL) and run as a batch function. Following batch analysis, the quality of image segmentation was confirmed visually to ensure accurate segmentation. If batch parameters were not sufficient, they were adjusted on a case-by-case basis and the segmentation analysis was rerun. For TUNEL analysis, the number of puncta (observed as objects) was calculated per image and averaged to obtain an average number per replicate. Individual averages for each developmental stage grouping were averaged together and plotted to generate graphs. For Sox10 nuclei counting, a further adjustment was made to accurately account for all nuclei in an image. After the segmentation was run, two values were found: the median area of nuclear objects and the total area of all objects. The total area was divided by the median nuclei size to generate an adjusted nuclei count. The adjusted count was found per image and averaged to obtain an average number per replicate. Individual averages for each developmental stage grouping were averaged together and plotted to generate graphs.

Neuron branching: Z-stack images of the OpV branch of the trigeminal ganglion were analyzed in ImageJ using custom ImageJ Macro language (IJM) scripts (available upon request). Maximum intensity Z-projection images were saved as an 8-bit image. Each image was input into the ImageJ macro as an 8-bit image where the user was prompted to broadly and manually create a closed polygon selection that encompassed the entire ophthalmic branch of interest and its distal neuronal extensions. Once the region of interest was selected, the ImageJ macro iterated over the entirety of the image with a vertical line selection and ran the command, *getProfile()* at 30μm intervals. Results were exported at each interval and served as input into a separate script created in R (R core team, Vienna, Austria, 2021) using the R programming language (available upon request).

The peaks obtained via *getProfile()* at each interval across an image identified unique neuronal branches. To identify individual peaks in each iteration, the *smooth.spline()* function was used in base R to fit a curve with known maxima and minima to the profile outputted from the ImageJ macro in each iteration. A subsequent results

387 table was produced for each image documenting the number of maxima at 30μm intervals
388 from the sample edge. Data were transformed, if necessary, so that for all images
389 assessed, increasing distance from baseline represented an increased distance from the
390 trigeminal ganglion. Data for individual replicates for each condition were aligned in
391 PRISM (GraphPad Software, Inc.) so that quantification of neuronal branching over a
392 distance concordantly began with the first measurement found. Data were displayed as
393 the mean quantity of neuronal branches ± SEM and plotted to generate graphs.
394 **Bundle width:** Using maximum intensity Z-projections, bundle width
395 measurements for both the lateral and medial nasal nerves were generated using the
396 straight line tool on FIJI. The diameter of individual nerve bundles (prior to the point where
397 nerve fascicles branched into individual neurons) were measured based on Tubb3 signal
398 and summed together to yield one value per embryo. Individual bundle widths were
399 averaged together for N-cadherin MO-treated embryos and their contralateral control
400 sides and plotted to generate graphs.
401 **Innervation area:** Using maximum intensity Z-projections, innervation area
402 measurements for both the lateral and medial nasal nerves were generated using the
403 polygon tool on FIJI. A border was drawn around the Tubb3 signal following extensive
404 neuron branching. Individual area measurements were averaged together for N-cadherin
405 MO-treated embryos and their contralateral control sides and plotted to generate graphs.
406 **Explant analysis**: Each low magnification, tiled image of the explants was first
407 converted to 8-bit images on FIJI. Using the polygon function, the explant tissue piece,
408 as well any background signal not associated with axons, was cleared for the images.
409 Next, the ridge detection plug-in was used to highlight neurons to obtain median axon
410 length and the detected segment version of the image was saved. Using the detected
411 segment images and the concentric circle plugin, 20 concentric circles were overlayed on
412 the images, with the center circle being placed in the center of the explant. The number
413 of axonal intersections across each circle of increasing diameter was counted and
414 compiled into a spreadsheet where the averages ± SEM were plotted in 175μm intervals.
415
416

RESULTS

N-cadherin knockdown in placode cells disrupts trigeminal ganglion development

While the expression of N-cadherin in cranial placode cells as well as sensory and motor neurons has been established[51–54], along with N-cadherin function in early trigeminal ganglion assembly[38], the role of N-cadherin in later trigeminal ganglion development in both placode cell- and neural crest cell-derived neurons is unknown. To elucidate the function of N-cadherin-expressing placodal neurons in the formation and maturation of the trigeminal ganglion, a validated N-cadherin morpholino (MO) was unilaterally electroporated into trigeminal placode cells prior to their delamination[38]. The electroporated embryos were grown for up to five days post-electroporation and assembled into stage groupings based on 24-hour increments. Trigeminal ganglion and nerve morphology was analyzed following whole-mount immunohistochemistry with an antibody to Tubb3 to label neurons and tissue clearing to render samples transparent for imaging. Based on previous literature[15,30], the majority of neural crest cells begin differentiating and contributing to the neuronal population of the trigeminal ganglion beginning at E5, with some differentiating earlier at E4. Therefore, up to E4, it is assumed that the Tubb3 antibody is only labeling placode cell-derived neurons, and after labels neuronal contributions from both cell types indistinguishably.

During initial gangliogenesis (Figure 1A-A', E2.5), N-cadherin depletion from trigeminal placode cells leads to increased dispersal of neurons (Figure 1E) due to the inability of placodal neurons to properly intermix with undifferentiated neural crest cells. These results recapitulate what has been shown previously in that perturbation of N-cadherin during early gangliogenesis impacts proper aggregation of trigeminal placodal neurons[38]. Following the condensation of the trigeminal ganglion 24 hours later, placodal neurons can assemble into the forming trigeminal ganglion; however, surprisingly, the opposite phenotype is now observed. We note a statistically significant reduction in the size of the trigeminal ganglion on the electroporated side (Figure 1B-B', E, E3.5) compared to the contralateral control (untreated side) of the same embryo (and to control MO-treated embryos, Supplemental Figure 1). One day later (Figure 1C-C', E4.5), as neural crest cells start differentiating into neurons, the reduction of the trigeminal ganglion persists and it is significantly smaller (Figure 1E). Although the trigeminal ganglia that

448 were electroporated are visually still smaller at E5.5, they no longer show statistically
449 significant differences in area (Figure 1E). Lastly, at E6.5, the surface area between the
450 contralateral control and the electroporated trigeminal ganglia are not significantly
451 different (data not shown, Figure 1E).

452 Following the results from the whole trigeminal ganglion surface area
453 measurements, we next sought to discern whether N-cadherin had differential importance
454 within the OpV and the MmV placodes, seeing as these placodes arise distinctly from one
455 another[12,13]. Thus, surface area measurements were repeated, this time separately
456 measuring the OpV and MmV lobes and nerves from the trigeminal ganglion.
457 Interestingly, N-cadherin knockdown leads to a statistically significant increase in
458 dispersal of MmV neurons, with no impact to OpV neurons, at E2.5 when the ganglion is
459 beginning to assemble (Figure 1F, G). However, after condensation (E3.5-E5.5), N-
460 cadherin depletion did not impact the MmV lobe (Figure 1G) but did lead to a statistically
461 significant reduction in OpV lobe size (Figure 1F), correlating with what we observed
462 qualitatively. At E6.5, the size of both lobes was approximately the same. Given the drastic
463 effects of N-cadherin knockdown on OpV compared to MmV (Figure 1F, G), we chose to
464 focus on the development of the OpV lobe in subsequent experiments.
465

466 **N-cadherin knockdown in placode cells does not lead to changes in cell death or**
467 **the number of neural crest cells within the trigeminal ganglion**

468 To assess whether the decreased size of the trigeminal ganglion was due to an
469 increase in cell death and/or a change in the contribution of neural crest cells, a TUNEL
470 assay and Sox10 immunohistochemistry, respectively, were performed on tissue sections
471 take through the trigeminal ganglion. Only the stage groupings that showed significant
472 differences in size from Figure 1 were examined (HH16-18, HH19-22, HH23-25). These
473 experiments revealed no differences in cell death or the number of neural crest cells
474 between the contralateral side of the embryo (Figure 2A-A'''') and the N-cadherin MO-
475 treated side (Figure 2B-B''', C, D). Apoptosis within the trigeminal ganglion was evident
476 on both the contralateral control (Figure 2A') as well as the N-cadherin MO (Figure 2B')
477 side, with no significant differences in the amount of TUNEL signal between the two
478 (Figure 2C). Furthermore, there is little co-localization of MO-positive cells and the TUNEL

479 signal, indicating that MO-expressing cells are not dying (Figure 2B', arrowheads). When
480 examining TUNEL distribution, the TUNEL signal did not preferentially co-localize with
481 either Tubb3 (marking neurons; Figure 2A", B"), or Sox10 (marking undifferentiated neural
482 crest cells and newly differentiated glia).

483 Intriguingly, these data revealed less overall cell death occurring in the first stage
484 grouping (initial trigeminal ganglion assembly) compared to the later stage groupings.
485 Following condensation during these later stage groupings, however, it does not appear
486 that there is a trend in the amount of cell death, as the average number of TUNEL-positive
487 cells is not significantly different between the HH19-H22 and H23-H25 group (Figure 2C).
488 Regarding the number of Sox10-positive nuclei present within the trigeminal ganglion
489 after N-cadherin knockdown, there is also no statistically significant difference between
490 the contralateral control and the electroporated sides (Figure 2D). These results indicate
491 that the decrease in trigeminal ganglion size is not due to increased cell death or a
492 reduction in the number of neural crest cells present in the trigeminal ganglion.

493

494 **Depletion of N-cadherin from trigeminal placode cells disrupts OpV target**
495 **innervation by the lateral nasal branch**

496 Our TUNEL and Sox10 data suggest there is no impact on the neuron cell body
497 and glial contribution to the ganglion upon N-cadherin knockdown in placode cells. As
498 such, we sought to discern whether the neuronal projections, or axons, to target tissues
499 might be impacted instead. We first examined the lateral nasal branch, one of the nerve
500 branches of the OpV lobe, at embryonic stage group HH23-25, as by this point, the branch
501 is a prominent structure within the embryonic head[55]. To this end, we used whole-mount
502 immunohistochemistry with an antibody to Tubb3, which labels both placodal and neural
503 crest-derived neurons at this stage. These experiments revealed a substantial reduction
504 in the axons of this branch after N-cadherin MO treatment (Figure 3A-A'). The
505 corresponding nerve on the contralateral control side appeared to have more nerve
506 bundles as well as individual axons growing towards the rostral side of the embryo (Figure
507 3A), while the experimental side often had only one nerve bundle and many fewer
508 individual axons (Figure 3A').

To quantify this apparent decrease in nerve outgrowth, the number of axons was counted at 30μm intervals across each image for the contralateral and experimental sides. While initially there is no significant change between the groups, as the main axon bundle splits into smaller bundles, there are significant reductions on the N-cadherin MO-treated side (Figure 3B). Next, bundle width and innervation area were also measured to evaluate fasciculation (Figure 3C) and target innervation (Figure 3D), respectively. For both bundle width and innervation area, the values were significantly reduced after N-cadherin knockdown, indicating that N-cadherin is needed not only for proper nerve outgrowth and fasciculation, but also for at least some of the individual neurons to send axons to their targets (Figure 3C, D).

Depletion of N-cadherin from trigeminal placode cells leads to specific defects in OpV innervation by the medial nasal nerve

Next, we examined another branch of the OpV lobe, the medial nasal branch, using the same types of analyses performed in Figure 3. Although the medial nasal nerve is beginning to form in HH23-25 staged embryos[55], there was more variability in the development of this branch during these stages of development. Therefore, we chose to examine the HH26-27 stage grouping due to more consistent morphological development among embryos. Again, whole-mount immunohistochemical staining with Tubb3 revealed a decrease in axonal projections between the control and experimental sides of the embryos (Figure 4A-A'), indicating that N-cadherin is likely needed in a similar manner for these branches of the OpV lobe. Interestingly, when the axon branches were counted between the two groups, there was no significant difference at any point (Figure 4B). Furthermore, both bundle width and innervation area were decreased for this branch, in keeping with the results from the lateral nasal branch (Figure 4C, D). For both measurements, the medial nasal branch was impacted to lesser extents compared to the lateral nasal nerve (bundle width $p=0.0009$ for lateral vs $p=0.0055$ for medial, innervation area: $p=0.0029$ for lateral vs $p=0.0374$ for medial). These results reveal that N-cadherin controls the proper development of at least some nerve branches of the OpV lobe in distinct ways.

540 **N-cadherin is important for proper axon outgrowth of trigeminal neurons *in vitro***

541 Given the phenotypes observed *in vivo* that could not be attributed to changes in
542 cell number, we hypothesized that trigeminal axon outgrowth was facilitated by N-
543 cadherin in an adhesion-dependent manner. If trigeminal neurons were expressing less
544 N-cadherin, they may not be adhering to each other as well and would not be able to grow
545 out as effectively, leading to reduced outgrowth and target innervation. To test this, we
546 chose to utilize a function-blocking antibody against the extracellular domain of N-
547 cadherin, known as MNCD2[54,56], and test our hypothesis *in vitro* using explanted
548 trigeminal ganglion tissue. Explants were cultured *in vitro*, treated with MNCD2 or a rat
549 IgG control antibody for 24 hours, followed by Tubb3 immunocytochemistry and analysis.
550 Qualitatively, more axons appeared to grow out in control explants (Figure 5A) compared
551 to MNCD2-treated explants (Figure 5A'). Further processing of images was then
552 performed to detect individual axons (Figure 5B-B'), and then a modified intersection
553 analysis was run to measure changes to axon outgrowth (Figure 5C-C'). We discovered
554 a significant reduction to the amount of Tubb3 signal in the MNCD2-treated samples
555 (Figure 5D), indicating fewer trigeminal neurons after blocking N-cadherin adhesion.
556 Furthermore, our intersection analysis showed diminished axonal intersections overall
557 within the MNCD2-treated explants, pointing to reduced axonal outgrowth and complexity
558 (Figure 5E). Interestingly, when looking at the median length of a single axon between
559 the two treatments, there was no significant difference (Figure 5F). This indicates that
560 some trigeminal neurons are not dependent on N-cadherin and can properly grow out to
561 the periphery in the absence of N-cadherin. Taken together, these findings reveal that
562 blocking the adhesive function of N-cadherin reduces the overall outgrowth of some, but
563 not all, trigeminal neurons.
564
565

566 **DISCUSSION**

567 During neurodevelopment, cells experience several environmental changes as
568 they migrate to their terminal locations and differentiate into specialized neurons. The first
569 neurons to grow to target tissues, termed pioneers, set the path that all later born neurons
570 will use as a template. Here we demonstrate a sustained role for N-cadherin during
571 trigeminal gangliogenesis that shows the importance of this cell adhesion molecule during
572 the formation and maturation of the trigeminal ganglion as it innervates its target tissues.
573 Our findings show that reducing N-cadherin from trigeminal placode cells and their
574 neuronal derivatives leads to defects in overall trigeminal ganglion morphology and
575 negatively impacts the lateral and medial nasal branches of the ophthalmic lobe.
576 Intriguingly, these phenotypes cannot be attributed to increased apoptosis or changes to
577 the number of neural crest cells present within the trigeminal ganglion. We have found
578 that N-cadherin-mediated adhesion is necessary for the outgrowth of the majority but not
579 all trigeminal neurons. Our results suggest that a subpopulation of placodal neurons serve
580 as the pioneers for the trigeminal ganglion and function independently of N-cadherin,
581 while the remaining follower neurons of both cellular origins rely on N-cadherin for proper
582 outgrowth and target innervation.

583

584 **Depletion of N-cadherin in placodal neurons leads to morphological defects of the**
585 **trigeminal ganglion at certain developmental timepoints**

586 Although a role for N-cadherin-expressing placode cells has been shown during
587 the coalescence of neural crest and placodal neurons as they initially generate the
588 trigeminal ganglion[57], how these early N-cadherin-expressing neurons impact trigeminal
589 gangliogenesis, and the ability of the trigeminal ganglion to properly innervate its targets
590 as embryogenesis progresses, is not understood. We first sought to understand whether
591 the phenotypes reported during early gangliogenesis[57] influenced trigeminal ganglion
592 morphology at later developmental stages. Using relative surface area measurements we
593 found that during early gangliogenesis N-cadherin knockdown leads to increased
594 dispersal of trigeminal neurons and a larger surface area than controls, replicating
595 previously published results[57]. Although there is increased dispersal of trigeminal neurons
596 during early gangliogenesis, these neurons are eventually able to coalesce to form the

597 trigeminal ganglion as development progresses. Interestingly, once cells condense, N-
598 cadherin MO-treated trigeminal ganglia were significantly smaller up to 4.5 days into
599 development. At both 5.5 and 6.5 days, there were no statistical differences between the
600 N-cadherin knockdown and control groups when looking at the entire trigeminal ganglion.
601 We believe there are two likely reasons for this trend. First, MOs are typically only stable
602 for up to 4-5 days *in vivo*, reflecting a limitation of our technique[58]. Therefore, it is possible
603 that at the later stages that were examined, the MO was getting degraded, leading to
604 reduced phenotypic effects. This is further supported by the presence of MO-positive
605 puncta in the cytoplasm of placodal neurons, representing vesicles like lysosomes (not
606 shown). Second, it is possible that (additional) neural crest cells differentiate into neurons
607 between E4-5[2] to compensate for effects on placodal neurons after N-cadherin
608 knockdown.

609 The placode contribution of the trigeminal ganglion can be separated into two
610 distinct placodes, the ophthalmic and the maxillomandibular. While both placodes will give
611 rise to placodal neurons within the trigeminal ganglion, they express specific markers and
612 undergo differentiation at different times[59,60]. Ophthalmic placode cells express neuron-
613 specific markers earlier than maxillomandibular placode cells, and there is evidence that
614 a subset of ophthalmic placode cells differentiate and become post-mitotic while still in
615 the ectoderm. Conversely, the majority of maxillomandibular placode cells remain as
616 neuroblasts until after delamination from the ectoderm. Additionally, previous work has
617 reported more drastic phenotypes in the OpV lobe compared to the MmV lobe after N-
618 cadherin knockdown in placode cells[57]. Taking this into consideration, we next chose to
619 separately measure the surface areas of the OpV lobe and MmV lobe to determine
620 whether the requirement for N-cadherin was different between the two placodes.
621 Interestingly, the results were near complete inverses of each other. While there was no
622 significant difference during the first stage grouping measured for the OpV lobe, this time
623 point was the only place that showed significant results for the MmV lobe. Although it is
624 possible that N-cadherin is differentially required in the two placodes as they have unique
625 origins, we hypothesize that this difference is most likely due to the MO getting diluted out
626 over time in MmV. These neuroblasts continue to undergo cell division before
627 differentiating into neurons and becoming post-mitotic, whereas the OpV placode cells

628 are either already post-mitotic or about to differentiate when the electroporation is
629 performed, leading to more discernable phenotypes. When analyzing the OpV lobe, we
630 noticed that E3.5 showed the greatest difference in size of all the time points measured.
631 Together with previous data, our results indicate that knockdown of N-cadherin does not
632 impact the ability of the placode cells to migrate to the location of the trigeminal ganglion[57],
633 nor does it lead to increased apoptosis that could explain the changes to size. This time
634 point represents when the majority of placodal neurons have initiated growth to their
635 target tissues[30], and therefore might explain why the phenotype is the most drastic at this
636 stage. If N-cadherin is needed by some placodal neurons for axon outgrowth, then its
637 reduction would provide a molecular explanation for the results we observed.
638

639 **Morphological changes after N-cadherin knockdown from placode cells cannot be**
640 **attributed to increased cell death or changes to neural crest cells within the**
641 **trigeminal ganglion**

642 Given the changes to trigeminal ganglion morphology observed upon N-cadherin
643 depletion from placode cells, we next sought to discern whether these phenotypes were
644 due to changes in the number of cells present within the trigeminal ganglion. As depletion
645 of N-cadherin from placode cells does not impact ingression[57], we sought to evaluate the
646 other critical cell population, the neural crest, and cell death in the trigeminal ganglion. To
647 this end, we examined the number of neural crest cells and apoptosis, one or both of
648 which could also decrease the size of the trigeminal ganglion. Our results indicate no
649 change in the number of neural crest cells within the trigeminal ganglion nor no increase
650 in apoptosis within the trigeminal ganglion after N-cadherin knockdown. The TUNEL
651 signal did not preferentially co-localize with MO-positive cells and neural crest and
652 placode cells were equally apoptotic, supporting the notion that one cell type is not
653 undergoing more apoptosis than the other during trigeminal gangliogenesis. Therefore,
654 apoptosis is not a driving factor behind the reduction in size of the trigeminal ganglion
655 after N-cadherin knockdown. Interestingly, we observed that the majority of TUNEL signal
656 was found adjacent to Sox10-positive nuclei, which may be identifying future glial cells.
657 This phenomenon, seen previously[61,62] suggests that glial cells aid in the removal of
658 debris during gangliogenesis. When looking at general trends of cell death occurring

659 within the trigeminal ganglion over development, the first time point had decreased
660 apoptosis compared to the other two time points. This can be explained by the presence
661 of a larger number of neurons initially that decreases over time as trigeminal neurons
662 receiving target-derived growth factors specialize and differentiate, while the ones that do
663 not eventually perish[63]. Given this, we anticipate observing more cell death in the embryo
664 at later stages.

665 Due to the reciprocal manner in which placodal neurons and neural crest cells
666 engage with each other, it was important to examine potential changes to neural crest cell
667 number, as it was possible that disrupting a cadherin on one cell type could impact the
668 interactions with the other cell type. However, our results showed no difference to the
669 number of neural crest cells at any of the stages examined. When evaluating the overall
670 number of Sox10-positive cells within the trigeminal ganglion, we noticed a steady
671 increasing trend as the embryo progressed through development. This represents the
672 continued contribution of undifferentiated migratory neural crest cells to the ganglion and
673 their eventual differentiation into neurons (Sox10-negative) and glia (Sox10-positive). It is
674 important to note that we did not examine much later stages of trigeminal gangliogenesis
675 when more neurons within the trigeminal ganglion would be neural crest-derived. As
676 neural crest cells turn off Sox10 once they have differentiated into neurons, it is likely that
677 the number of Sox10-positive cells would decrease at later stages of development, as it
678 would then only mark glial cells.

679

680 **Reducing N-cadherin from placodal neurons impacts OpV nerve branch**
681 **innervation to target tissues**

682 Traveling away from the cell bodies housed in the trigeminal ganglion, we next
683 sought to understand how N-cadherin knockdown from placodal neurons impacted axonal
684 outgrowth to target tissues. We chose to examine two branches of the OpV lobe, the
685 lateral and medial nasal nerve branches. Although both branches arise from the cell
686 bodies of the OpV lobe, we found that N-cadherin is needed in different manners between
687 the two, with the lateral medial branch exhibiting more drastic changes. When examining
688 the number of axons traveling to target tissues through intersection analyses, we found
689 there were multiple points that were significantly reduced for the lateral nasal branch.

690 Additionally, we observed a decrease in bundling of the nerve prior to extensive branching
691 and a reduction in innervation area. While the medial nasal nerve exhibited similar trends
692 for bundle width and innervation area, albeit to a lesser degree, the results from the
693 intersection analysis were not changed at any of the points measured. This contrasting
694 result - a smaller nerve bundle having similar axonal branching - suggests that N-cadherin
695 functions to adhere individual axons at targets to each other for the medial nasal branch
696 of OpV. Similar phenotypes after N-cadherin perturbations have been observed in other
697 systems as well[53,64,65].
698 Although both of these branches begin developing a similar stages during
699 development[55] we noticed much more variation in the medial nasal nerve in the HH23-25
700 embryo group. To this end, we chose to examine the next group, HH26-27, for more
701 consistency among the embryos. While it is possible that the difference in the stage of
702 embryo examined between the two nerve branches could explain the differences in
703 significance, we believe it is equally plausible that N-cadherin-expressing placodal
704 neurons are needed to different extents in the two branches. Since the contribution of
705 neural crest-derived neurons and placodal neurons has not been examined for these
706 nerve branches before, it is possible that neural crest- and placode-derived neurons
707 comprise the bulk of the medial nasal and lateral nasal nerves, respectively. Another
708 potential explanation for the differences observed between the nerves could be due to
709 when the branches develop. Our results suggest that the medial nasal branch develops
710 slightly later than the lateral nasal branch. If this is true, then the early knockdown of N-
711 cadherin could preferentially impact nerve branches developing earlier versus later.
712 While the majority of embryos analyzed showed reduction to the nerve branches,
713 a subset of embryos actually showed increased measurements for bundle width and
714 innervation area measurements due to increased nerve bundles and increased individual
715 axons at targets. This suggests that while the overt phenotype of N-cadherin knockdown
716 leads to a reduced ability of axons to grow along other neurons and properly reach
717 targets, a subset of neurons, potentially the earliest ones to extend axons, is still able to
718 grow. However, these neurons, also lacking N-cadherin, cannot adhere to surrounding
719 axons in a proper manner, leading to these phenotypes.
720

721 **Homophilic N-cadherin-mediated interactions facilitate the outgrowth of some**
722 **trigeminal neurons**

723 To understand whether the phenotypes seen *in vivo* were due to an adhesion-
724 dependent role of N-cadherin during trigeminal gangliogenesis, we chose to utilize a
725 function-blocking antibody that binds to the extracellular domain of N-cadherin and
726 prevents its interactions with other cadherins. Multiple conditions, including concentration
727 of antibody and incubation times of explants, were tested prior to beginning
728 experimentation. We chose a concentration of MNCD2 that showed phenotypic changes
729 to the explants without eliciting cellular responses indicative of apoptosis. Additionally, we
730 noted that regardless of the incubation time of the explants prior to incorporating the
731 MNCD2 antibody into the media, there was some axon outgrowth occurring. This
732 suggests that some trigeminal axons are dependent on N-cadherin for outgrowth, while
733 others are not.

734 Analysis of the N-cadherin function-blocking *in vitro* experiments led to three major
735 conclusions. First, overall, fewer trigeminal neurons are able to migrate out of the explant
736 and towards the periphery of the dishes in which they were grown. This was evident both
737 visually as well as when the fluorescent intensity of each image was measured. Second,
738 and in line with this, our intersection analyses indicate reduced outgrowth and less
739 branching of neurons when N-cadherin adhesion is abrogated. Lastly, when looking at
740 individual axon lengths, there were no significant differences in the median (and average,
741 not shown) axon length when comparing rat IgG control-treated explants to MNCD2-
742 treated explants. This result indicates that the subset of trigeminal neurons that are
743 unaffected by blocking N-cadherin function are reaching the periphery of the explants in
744 the same manner as their control counterparts, suggesting N-cadherin is not important
745 for the outgrowth ability of these neurons. This conclusion models what was observed *in*
746 *vivo* when examining target innervation by the lateral and medial nasal nerve branches.
747 In both instances, N-cadherin knockdown did not completely inhibit target innervation but
748 instead reduced the number of axons successfully reaching target tissues. While this
749 phenotype could be attributed to the mosaic nature of the MO electroporation, our *in vitro*
750 results now offer another explanation, in that some neurons are not reliant on N-cadherin
751 for their outgrowth.

752 Altogether, these findings reveal that some trigeminal axons rely on N-cadherin-
753 mediated adhesion to facilitate their outgrowth to targets, and mirrors what was observed
754 *in vivo* when N-cadherin was reduced from placodal neurons. We hypothesize that the
755 neurons that do not rely on N-cadherin are the true pioneers of the trigeminal ganglion.
756 These neurons, which migrate through surrounding tissues using guidance cues, appear
757 to be less reliant on cell adhesion compared to followers, which commonly utilize cell
758 adhesion molecules to grow along axon tracts established by the pioneers[66].
759 Furthermore, the cranial mesenchyme is also known to express N-cadherin[67], so it is
760 possible that interactions between neurons and surrounding cells also facilitate this
761 process. Patterned substrate assays for N-cadherin would be beneficial for addressing
762 this question.
763

CONCLUSION

In this study, we have shown a sustained negative impact on the trigeminal ganglion after N-cadherin is depleted from placodal neurons. Changes to the size of the trigeminal ganglion, as well as reduced axonal outgrowth to target tissues, are observed at early stages of development as well as later stages when neural crest cells have differentiated into neurons. These morphological changes cannot be explained by increased apoptosis or changes to neural crest cell number, suggesting an issue with the ability of neurons to properly grow out in the absence of N-cadherin. Blocking the extracellular domain of N-cadherin, which prevents the protein from interacting with other cadherins, leads to reduced axonal outgrowth, replicated results seen *in vivo*. Collectively, our results highlight a long-term, critical role for N-cadherin during trigeminal gangliogenesis.

794 **FIGURE LEGENDS**

795

796 **Figure 1. Knockdown of N-cadherin in placode cells disrupts trigeminal ganglion**
797 **development.** (A-D') Representative images of the lateral view of the chick embryo head
798 after immunostaining for Tubb3 and FRUIT (A-B') or iDISCO (C-D') clearing methods from
799 stage groupings (HH16-18: A-A' (n=10), HH19-22: B-B' (n=10), HH23-25: C-C' (n=14),
800 HH26-27: D-D' (n=13), not shown: HH28-30 (n=6)). Scale bar in (A) is 250μm and applies
801 to (A'-B'). Scale bar in (C) is 250μm and applies to (C'-D'). (E) Quantifications of relative
802 surface area of trigeminal ganglia taken from maximum intensity Z projections. (F)
803 Quantifications of relative surface area of only the OpV lobe taken from maximum
804 intensity Z projections. (G) Quantifications of relative surface area of only the MmV or
805 MxV/MnV taken from maximum intensity Z projections. Average surface areas were
806 graphed as histograms with error bars representing SEM. Arrowheads in (A'), (B'), (C'),
807 and (D') indicate reduction in OpV lobe size in N-cad MO samples compared to controls.
808 Paired t-tests were performed using GraphPad Prism and adjusted for multiple
809 comparisons. (*) $p<0.05$, (**) $p<0.01$, (***) $p<0.001$, (****) $p<0.0001$. Abbreviations: OpV:
810 ophthalmic; MmV: maxillomandibular; MxV: maxillary; MnV: mandibular; ns: not
811 significant.

812

813 **Figure 2. Morphology changes in the trigeminal ganglion after N-cadherin**
814 **knockdown in placode cells is not due to increased cell death or changes to neural**
815 **crest cells.** (A-B"') Transverse sections through the ophthalmic lobe of the trigeminal
816 ganglion from representative HH19 embryos with fluorescent immunohistochemistry for
817 Sox10 (blue, marks neural crest cells) and Tubb3 (purple, marks neurons) and TUNEL
818 staining (green, marks double stranded DNA breaks). Scale bar in (A) is 50μm and applies
819 to (B). Scale bar in (A') is 50μm and applies to (A", A"', B'-B"'). (C, D) Five serial sections
820 per embryo from stage groupings HH16-18 (n=6), HH19-22 (n=8), and HH23-25 (n=11)
821 were imaged and used for quantification analysis. ROIs were drawn to label the border of
822 the trigeminal ganglion using Tubb3 staining. Within each section, individual TUNEL-
823 positive cells and Sox10-positive nuclei were counted and averages were generated for
824 each embryo. Total average counts for stage groupings were graphed as histograms with

825 error bars representing SEM. Arrowheads in (B') mark MO-positive, TUNEL-negative
826 cells. Paired t-tests were performed using GraphPad Prism and adjusted for multiple
827 comparisons. Abbreviations: e, ectoderm; ns: not significant.
828
829 **Figure 3. N-cadherin depletion from placode cells negatively impacts lateral nasal**
830 **nerve outgrowth and target tissue innervation.** (A-A") Representative images of the
831 lateral view of chick embryo head following immunostaining for Tubb3 (marks neurons)
832 and clearing with iDISCO (n=12). Scale bar in (A) is 250μm and applies to (A'). (B) Axon
833 branch counts were generated using custom scripts on FIJI to measure the signal within
834 the ROI in 30μm intervals. Averages were plotted with error bars representing SEM. ** at
835 300μm, 420μm, 450μm, 480μm, and 510μm, **** at 330μm, 360μm, and 390μm. (C)
836 Bundle width was calculated as a summation of the width of the nerve bundle for each
837 embryo prior to extensive axon branching. Sums were averaged and plotted as
838 histograms with error bars representing SEM. (D) Innervation area of the Tubb3-positive
839 axons was calculated by measuring the ROI area where the axons terminate for each
840 embryo. Areas were averaged and plotted as histograms with error bars representing
841 SEM. A repeated measure ANOVA was used to calculate the statistical significance for
842 intersection analysis in (B) using GraphPad Prism. Paired t-tests were performed for (C,
843 D).
844
845 **Figure 4. N-cadherin knockdown in placode cells negatively impacts medial nasal**
846 **nerve outgrowth and target tissue innervation.** (A-A") Representative images of the
847 lateral view of chick embryo head following immunostaining for Tubb3 (marks neurons)
848 and clearing with iDISCO (n=13). Scale bar in (A) is 250μm and applies to (A'). (B) Axon
849 branch counts were generated using custom scripts on FIJI to measure the signal within
850 the ROI in 30μm intervals. Averages were plotted with error bars representing SEM. ns
851 at any of the distances measured. (C) Bundle width was calculated as a summation of
852 the width of the nerve bundle for each embryo prior to extensive axon branching. Sums
853 were averaged and plotted as histograms with error bars representing SEM. (D)
854 Innervation area of the Tubb3-positive axons was calculated by measuring the ROI area
855 where the axons terminate for each embryo. Areas were averaged and plotted as

histograms with error bars representing SEM. A repeated measure ANOVA was used to calculate the statistical significance for intersection analysis in (B). Paired t-tests were performed for (C, D).

Figure 5. Blocking the extracellular domain of N-cadherin reduces trigeminal neuron axon outgrowth. (A-C') Work-flow process for *in vitro* analyses. (A-A') Representative images of trigeminal ganglion explants after treatment with either control rat IgG (n=7) or MNCD2 (n=9) antibody, respectively, followed by immunostaining for Tubb3 (marks neurons). Scale bar in (A) is 1mm and applies to (A'). (B-B') Generated images after ridge detection processing on FIJI for rat IgG or MNCD2 treated explants, respectively. (C-C') Processed images overlaid with concentric circle function to count the number of axonal intersections. (D) Mean gray values of explant images after rat IgG or MNCD2 treatment. Averages were plotted with error bars representing SEM. (E) Intersection analysis graph calculating the number of axonal intersections across concentric circles of increasing diameter after function-blocking experiments. Averages were graphed with error bars representing SEM. Intersections with statistical differences: * at 175μm, 350μm, and 700μm, ** at 525μm. (F) Median length of axons of each explant image after rat IgG or MNCD2 treatment. Averages were plotted with error bars representing SEM. Unpaired t-tests were run for all graphs, with adjusted made for multiple comparisons for (E).

Supplemental Figure 1. N-cadherin control MO-treated embryos show no alterations in trigeminal ganglion morphology. (A-A') Representative images of the lateral view of the chick embryo head after immunostaining for Tubb3 and iDISCO clearing from stage group HH23-25: n=4. Scale bar in (A) is 250μm and applies to (A'). (B) Quantifications of relative surface area of trigeminal ganglia taken from maximum intensity Z projections. Average surface areas were graphed as histograms with error bars representing SEM. A paired t-test was performed using GraphPad Prism. Abbreviations: OpV: ophthalmic; MmV: maxillomandibular; MM: mismatch control MO; ns: not significant.

886 **Figure 1. Knockdown of N-cadherin in placode cells disrupts trigeminal ganglion**
887 **development.**

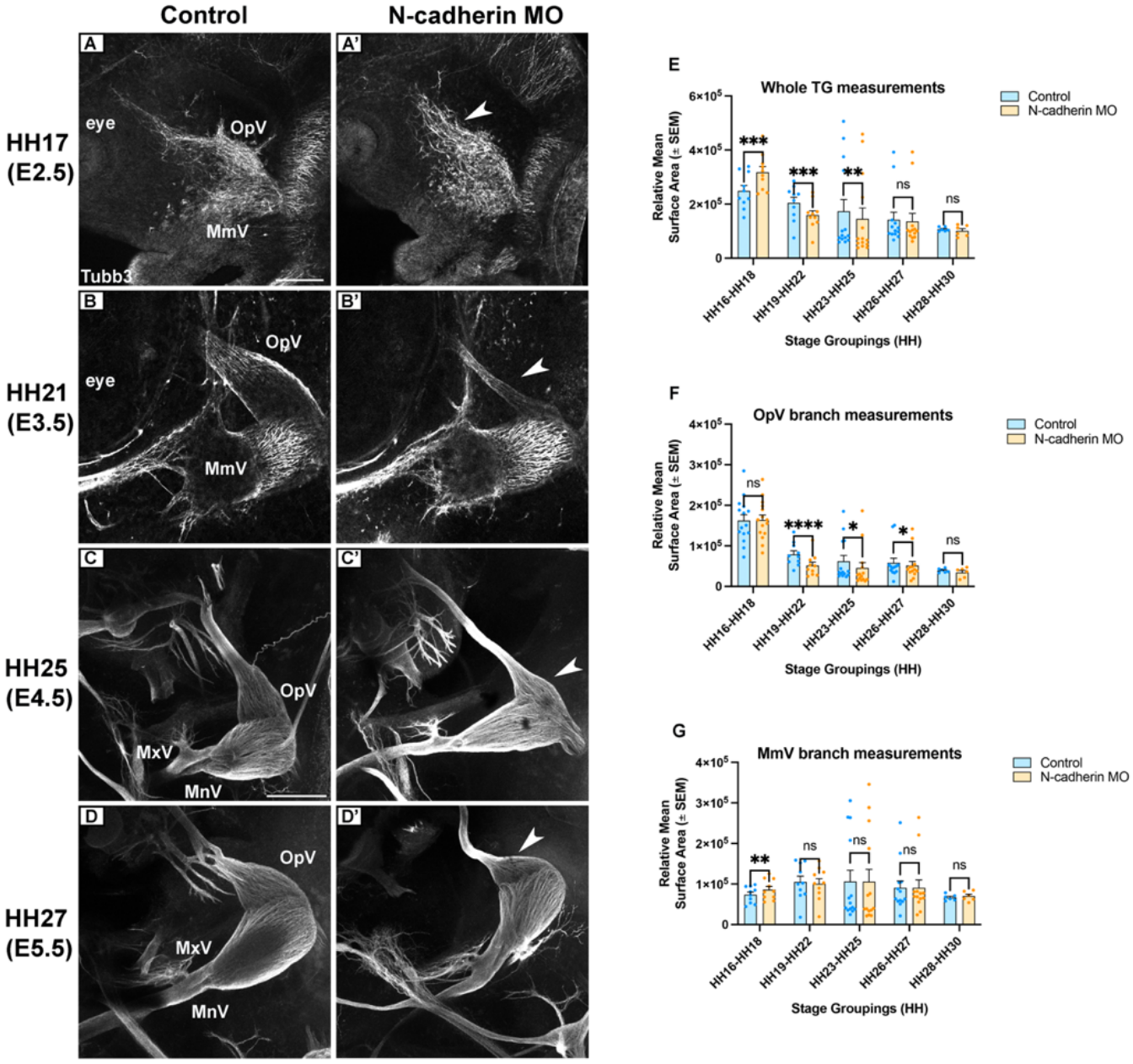

888
889
890
891
892
893
894

895 **Figure 2. Morphology changes in the trigeminal ganglion after N-cadherin knockdown in**
896 **placode cells are not due to increased cell death or changes to neural crest cells.**

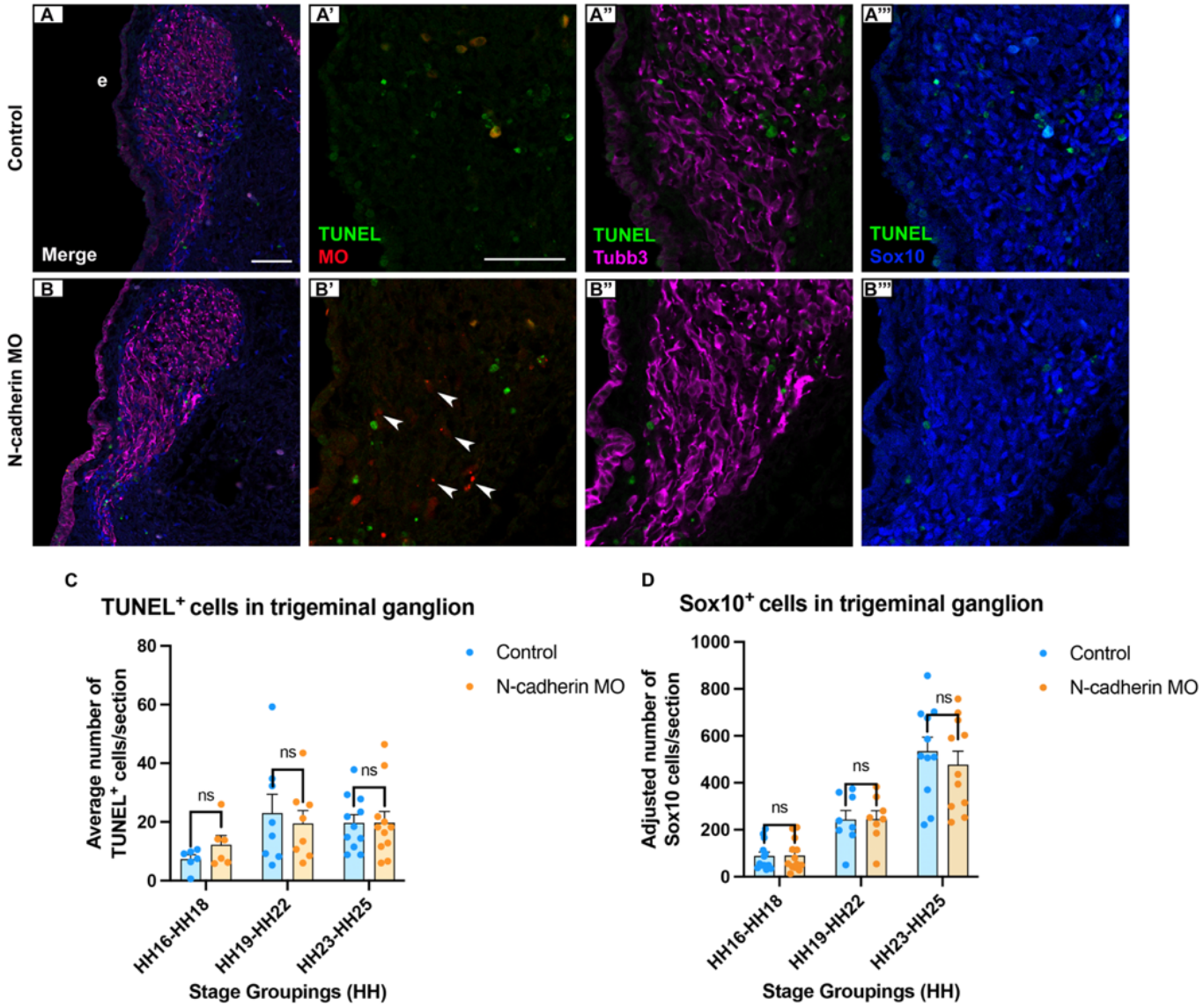

897
898
899
900
901
902
903

904 **Figure 3. N-cadherin depletion from placode cells negatively impacts lateral nasal nerve**
905 **outgrowth and target tissue innervation.**

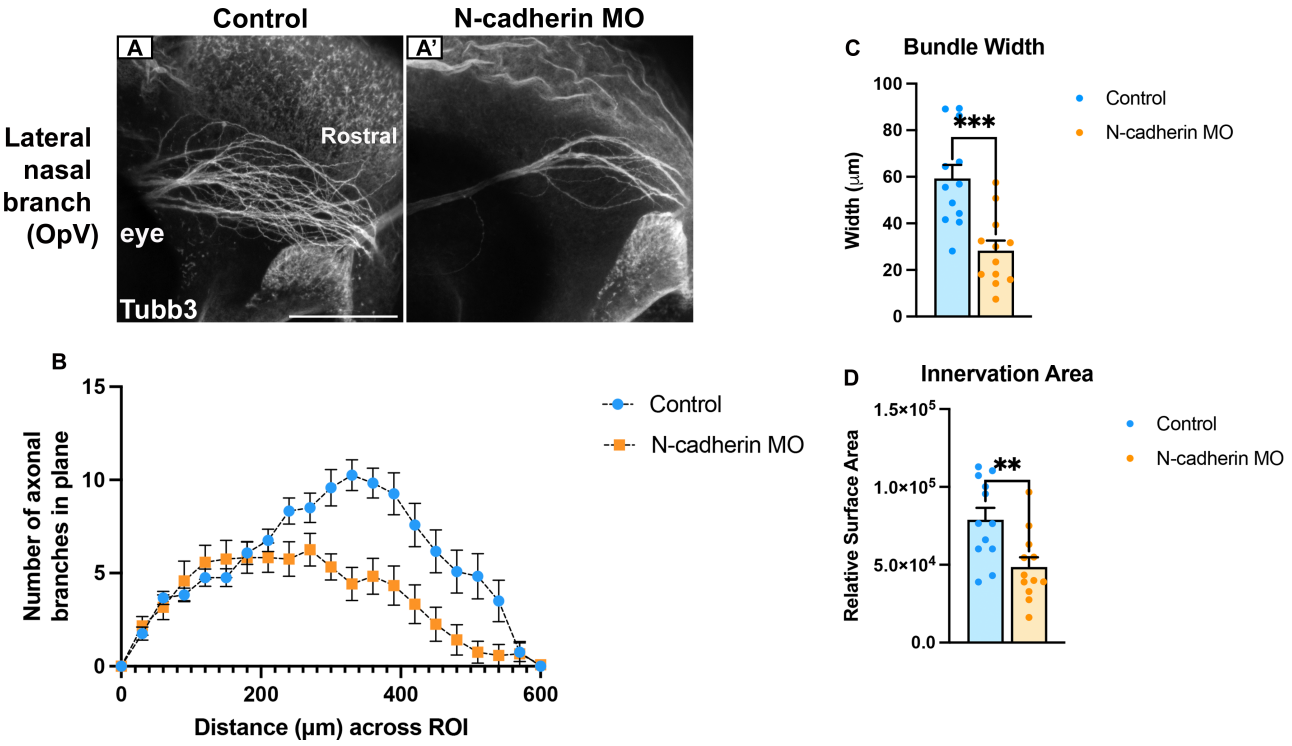

906
907
908
909
910
911
912
913
914
915
916
917
918
919

Figure 4. N-cadherin knockdown in placode cells negatively impacts medial nasal nerve outgrowth and target tissue innervation.

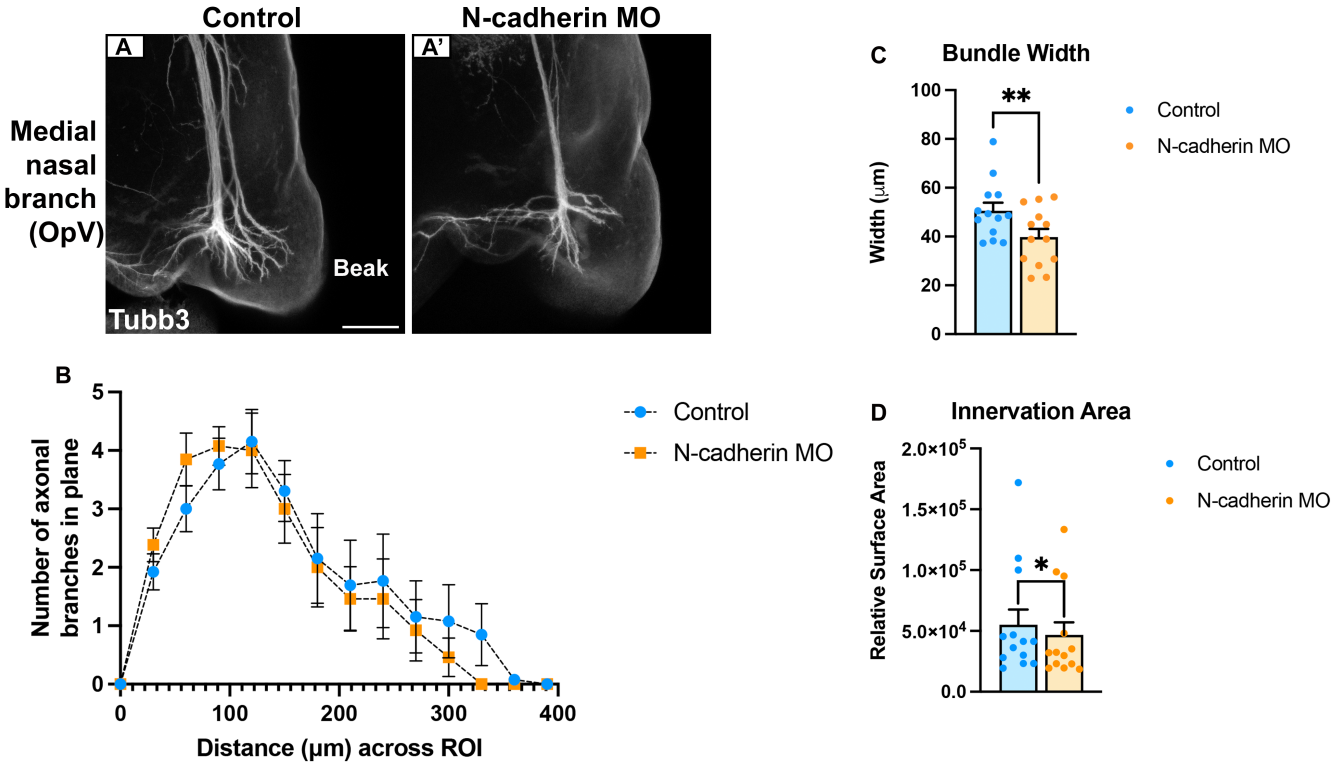

935 **Figure 5. Blocking the extracellular domain of N-cadherin reduces trigeminal neuron**
936 **axon outgrowth.**

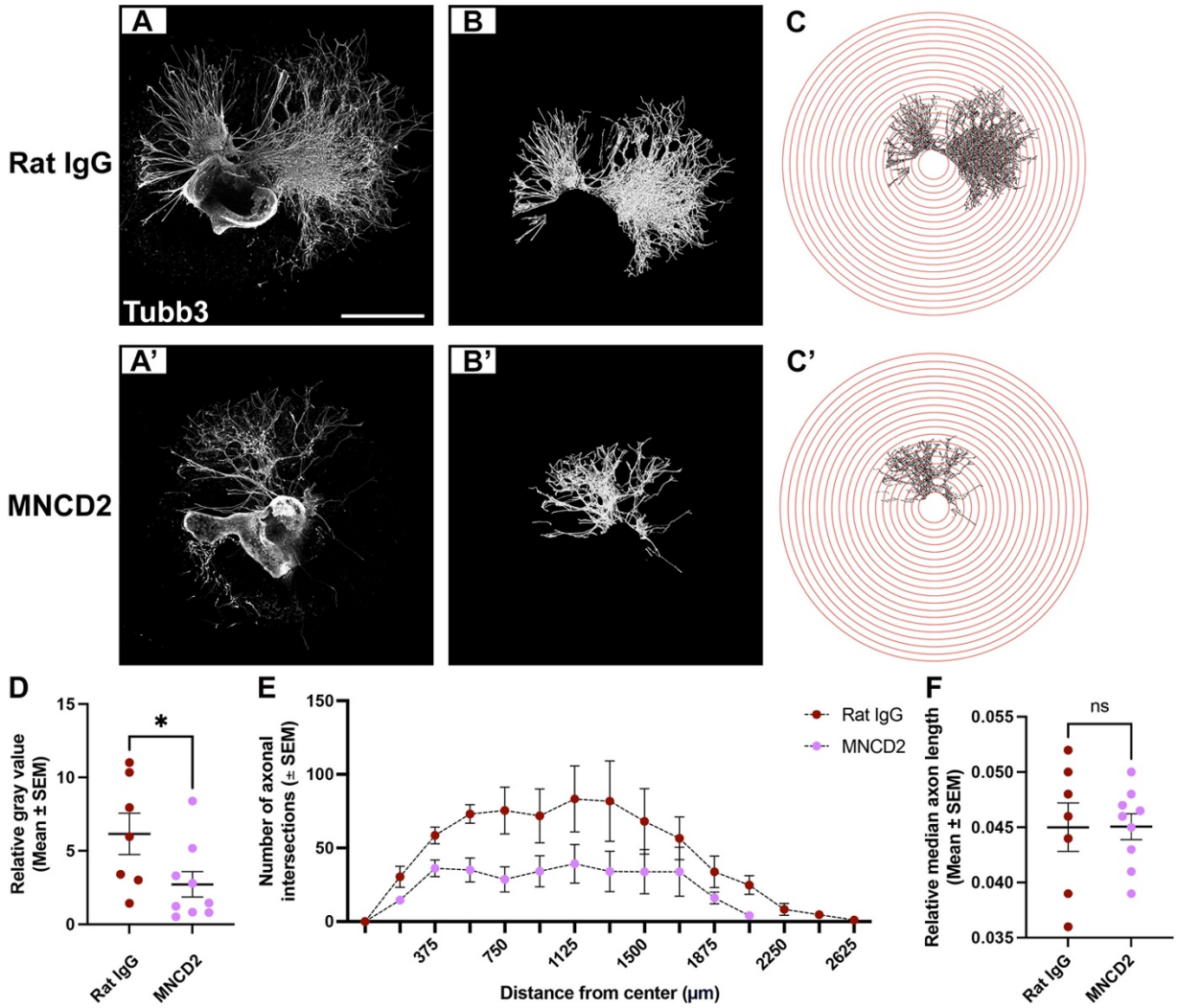

937
938
939
940
941
942
943
944
945
946
947
948
949
950

951 **Supplemental Figure 1. N-cadherin control MO-treated embryos show no alterations in**
952 **trigeminal ganglion morphology.**

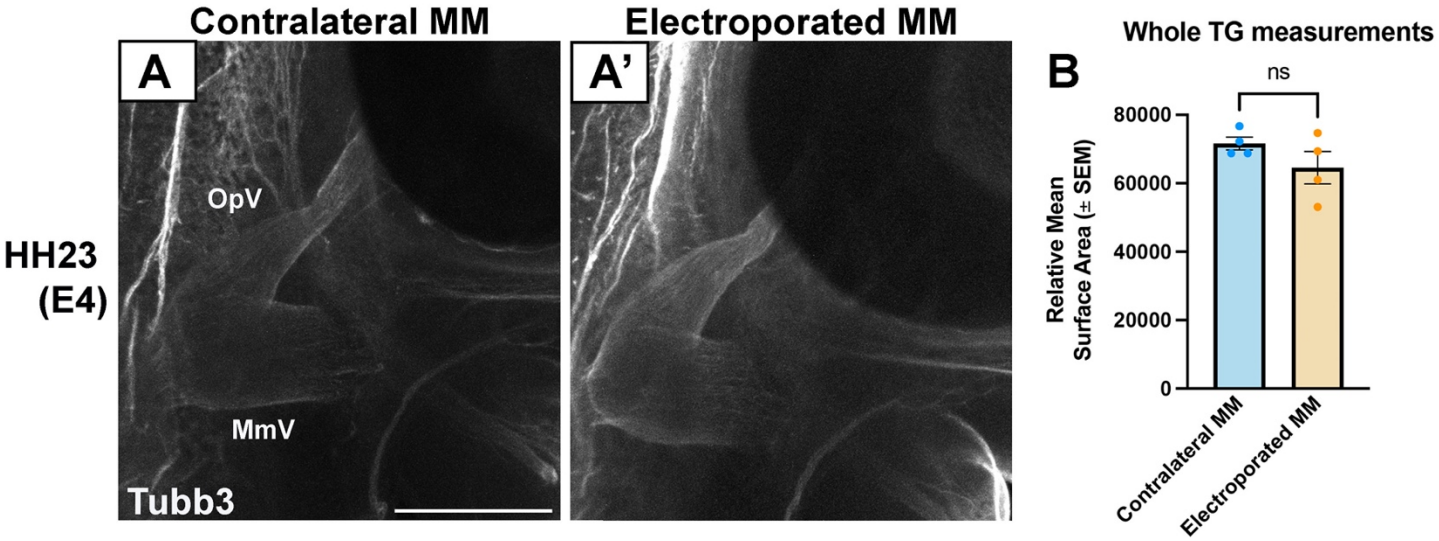

953
954
955
956
957
958
959
960
961
962
963
964
965
966
967
968
969
970
971
972
973
974

ACKNOWLEDGMENTS

The authors would like to thank the National Institute of Dental and Craniofacial Research (R01DE024217) and the University of Maryland Graduate School for financially supporting this research. Additionally, we would like to thank Ms. Zoe Davidson and Ms. Reagan Armstrong for their technical assistance.

REFERENCES

1. Hamburger, V. Experimental analysis of the dual origin of the trigeminal ganglion in the chick embryo. *J. Exp. Zool.* **148**, 91–123 (1961).
2. d'Amico-Martel, A. & Noden, D. M. An autoradiographic analysis of the development of the chick trigeminal ganglion. *J. Embryol. Exp. Morphol.* **55**, 167–182 (1980).
3. Dubey, A., Rose, R. E., Jones, D. R. & Saint-Jeannet, J. Generating retinoic acid gradients by local degradation during craniofacial development: One cell's cue is another cell's poison. *genesis* **56**, e23091 (2018).
4. Noden, D. M. The migratory behavior of neural crest cells. *Symp. Oral Sens. Percept.* 9–36 (1973).
5. Lumsden, A., Sprawson, N. & Graham, A. Segmental origin and migration of neural crest cells in the hindbrain region of the chick embryo. *Development* **113**, 1281–1291 (1991).
6. Rodrigues-Da-Silva, M. A., De Espindola Da Silveira, G., Taufer, C. R. & Calloni, G. W. The mesenchymal potential of trunk neural crest cells. *Int. J. Dev. Biol.* **66**, 317–331 (2022).
7. Shellard, A. & Mayor, R. Integrating chemical and mechanical signals in neural crest cell migration. *Curr. Opin. Genet. Dev.* **57**, 16–24 (2019).
8. Canales Coutiño, B. & Mayor, R. Neural crest mechanosensors: Seeing old proteins in a new light. *Dev. Cell* **57**, 1792–1801 (2022).
9. Schlosser, G. Making senses development of vertebrate cranial placodes. *Int. Rev. Cell Mol. Biol.* **283**, 129–234 (2010).
10. Bellairs, R. & Osmond, M. *The Atlas of Chick Development*. (Elsevier/AP, Academic Press is an imprint of Elsevier, Amsterdam, 2014).

1003 11. Graham, A. & Shimeld, S. M. The origin and evolution of the ectodermal placodes. *J.*
1004 *Anat*. **222**, 32–40 (2013).
1005 12. Begbie, J. Early Steps in the Production of Sensory Neurons by the Neurogenic Placodes.
1006 *Mol. Cell. Neurosci*. **21**, 502–511 (2002).
1007 13. McCabe, K. L., Sechrist, J. W. & Bronner-Fraser, M. Birth of ophthalmic trigeminal
1008 neurons initiates early in the placodal ectoderm. *J. Comp. Neurol*. **514**, 161–173 (2009).
1009 14. Shiau, C. E., Das, R. M. & Storey, K. G. An effective assay for high cellular resolution
1010 time-lapse imaging of sensory placode formation and morphogenesis. *BMC Neurosci*. **12**, 37
1011 (2011).
1012 15. D'amico-Martel, A. & Noden, D. M. Contributions of placodal and neural crest cells to
1013 avian cranial peripheral ganglia. *Am. J. Anat*. **166**, 445–468 (1983).
1014 16. Theveneau, E. *et al*. Chase-and-run between adjacent cell populations promotes
1015 directional collective migration. *Nat. Cell Biol*. **15**, 763–772 (2013).
1016 17. Breau, M. A. & Schneider-Maunoury, S. Cranial placodes: Models for exploring the
1017 multi-facets of cell adhesion in epithelial rearrangement, collective migration and neuronal
1018 movements. *Dev. Biol*. **401**, 25–36 (2015).
1019 18. Freter, S., Fleenor, S. J., Freter, R., Liu, K. J. & Begbie, J. Cranial neural crest cells form
1020 corridors prefiguring sensory neuroblast migration. *Dev. Camb. Engl*. **140**, 3595–3600 (2013).
1021 19. Moody, S. A. & Heaton, M. B. Developmental relationships between trigeminal ganglia
1022 and trigeminal motoneurons in chick embryos. I. Ganglion development is necessary for
1023 motoneuron migration. *J. Comp. Neurol*. **213**, 327–343 (1983).

1024 20. Shiau, C. E., Lwigale, P. Y., Das, R. M., Wilson, S. A. & Bronner-Fraser, M. Robo2-
1025 Slit1 dependent cell-cell interactions mediate assembly of the trigeminal ganglion. *Nat.*
1026 *Neurosci.* **11**, 269–276 (2008).
1027 21. Bate, C. M. Pioneer neurones in an insect embryo. *Nature* **260**, 54–56 (1976).
1028 22. Eisen, J. S., Myers, P. Z. & Westerfield, M. Pathway selection by growth cones of
1029 identified motoneurones in live zebra fish embryos. *Nature* **320**, 269–271 (1986).
1030 23. Ghosh, A., Antonini, A., McConnell, S. K. & Shatz, C. J. Requirement for subplate
1031 neurons in the formation of thalamocortical connections. *Nature* **347**, 179–181 (1990).
1032 24. Gong, Q. & Shipley, M. T. Evidence that pioneer olfactory axons regulate telencephalon
1033 cell cycle kinetics to induce the formation of the olfactory bulb. *Neuron* **14**, 91–101 (1995).
1034 25. Klose, M. & Bentley, D. Transient pioneer neurons are essential for formation of an
1035 embryonic peripheral nerve. *Science* **245**, 982–984 (1989).
1036 26. Lin, D. M., Auld, V. J. & Goodman, C. S. Targeted neuronal cell ablation in the
1037 drosophila embryo: Pathfinding by follower growth cones in the absence of pioneers. *Neuron*
1038 **14**, 707–715 (1995).
1039 27. Hidalgo, A. & Brand, A. H. Targeted neuronal ablation: the role of pioneer neurons in
1040 guidance and fasciculation in the CNS of *Drosophila*. *Development* **124**, 3253–3262 (1997).
1041 28. Clarke, A. *et al*. Dynamic morphogenesis of a pioneer axon in *Drosophila* and its
1042 regulation by Abl tyrosine kinase. *Mol. Biol. Cell* **31**, 452–465 (2020).
1043 29. Stainier, D. Y. & Gilbert, W. Pioneer neurons in the mouse trigeminal sensory system.
1044 *Proc. Natl. Acad. Sci. U. S. A.* **87**, 923–927 (1990).

1045 30. Moody, S. A., Quigg, M. S. & Frankfurter, A. Development of the peripheral trigeminal
1046 system in the chick revealed by an isotype-specific anti-beta-tubulin monoclonal antibody. *J.*
1047 *Comp. Neurol.* **279**, 567–580 (1989).
1048 31. Steventon, B., Mayor, R. & Streit, A. Neural crest and placode interaction during the
1049 development of the cranial sensory system. *Dev. Biol.* **389**, 28–38 (2014).
1050 32. Straub, B. K. *et al.* E–N-cadherin heterodimers define novel adherens junctions
1051 connecting endoderm-derived cells. *J. Cell Biol.* **195**, 873–887 (2011).
1052 33. Basu, R. *et al.* Heterophilic Type II Cadherins Are Required for High-Magnitude
1053 Synaptic Potentiation in the Hippocampus. *Neuron* **96**, 160-176.e8 (2017).
1054 34. Halmi, C. A., Wu, C.-Y. & Taneyhill, L. A. Neural crest cell-placodal neuron interactions
1055 are mediated by Cadherin-7 and N-cadherin during early chick trigeminal ganglion assembly.
1056 *F1000Research* **11**, 741 (2022).
1057 35. Niessen, C. M., Leckband, D. & Yap, A. S. Tissue organization by cadherin adhesion
1058 molecules: dynamic molecular and cellular mechanisms of morphogenetic regulation. *Physiol.*
1059 *Rev.* **91**, 691–731 (2011).
1060 36. Wu, C. & Taneyhill, L. A. Cadherin-7 mediates proper neural crest cell–placodal neuron
1061 interactions during trigeminal ganglion assembly. *genesis* **57**, e23264 (2019).
1062 37. Hatta, K. & Takeichi, M. Expression of N-cadherin adhesion molecules associated with
1063 early morphogenetic events in chick development. *Nature* **320**, 447–449 (1986).
1064 38. Shiau, C. E. & Bronner-Fraser, M. N-cadherin acts in concert with Slit1-Robo2 signaling
1065 in regulating aggregation of placode-derived cranial sensory neurons. *Dev. Camb. Engl.* **136**,
1066 4155–4164 (2009).

1067 39. Riehl, R. *et al*. Cadherin Function Is Required for Axon Outgrowth in Retinal Ganglion
1068 Cells In Vivo. *Neuron* **17**, 837–848 (1996).
1069 40. Masai, I. *et al*. N-cadherin mediates retinal lamination, maintenance of forebrain
1070 compartments and patterning of retinal neurites. *Development* **130**, 2479–2494 (2003).
1071 41. Benson, D. L. & Tanaka, H. N-Cadherin Redistribution during Synaptogenesis in
1072 Hippocampal Neurons. *J. Neurosci*. **18**, 6892–6904 (1998).
1073 42. Jontes, J. D., Emond, M. R. & Smith, S. J. *In Vivo* Trafficking and Targeting of N-
1074 Cadherin to Nascent Presynaptic Terminals. *J. Neurosci*. **24**, 9027–9034 (2004).
1075 43. Punovuori, K. *et al*. N-cadherin stabilises neural identity by dampening anti-neural
1076 signals. *Development* dev.183269 (2019) doi:10.1242/dev.183269.
1077 44. Aubert, J., Dunstan, H., Chambers, I. & Smith, A. Functional gene screening in
1078 embryonic stem cells implicates Wnt antagonism in neural differentiation. *Nat. Biotechnol*.
1079 **20**, 1240–1245 (2002).
1080 45. Hamburger, V. & Hamilton, H. L. A series of normal stages in the development of the
1081 chick embryo. *Dev. Dyn*. **195**, 231–272 (1992).
1082 46. Hou, B. *et al*. Scalable and DiI-compatible optical clearance of the mammalian brain.
1083 *Front. Neuroanat*. **9**, 19 (2015).
1084 47. Renier, N. *et al*. iDISCO: A Simple, Rapid Method to Immunolabel Large Tissue
1085 Samples for Volume Imaging. *Cell* **159**, 896–910 (2014).
1086 48. Schindelin, J. *et al*. Fiji: an open-source platform for biological-image analysis. *Nat*.
1087 *Methods* **9**, 676–682 (2012).
1088 49. Schneider, C. A., Rasband, W. S. & Eliceiri, K. W. NIH Image to ImageJ: 25 years of
1089 image analysis. *Nat. Methods* **9**, 671–675 (2012).

1090 50. Rizk, A. *et al*. Segmentation and quantification of subcellular structures in fluorescence
1091 microscopy images using Squassh. *Nat. Protoc*. **9**, 586–596 (2014).
1092 51. Itoh, K., Ozaki, M., Stevens, B. & Fields, R. D. Activity-dependent regulation of N-
1093 cadherin in DRG neurons: differential regulation of N-cadherin, NCAM, and L1 by distinct
1094 patterns of action potentials. *J. Neurobiol*. **33**, 735–748 (1997).
1095 52. Inuzuka, H., Redies, C. & Takeichi, M. Differential expression of R- and N-cadherin in
1096 neural and mesodermal tissues during early chicken development. *Development* **113**, 959–967
1097 (1991).
1098 53. Tan, Z.-J., Peng, Y., Song, H.-L., Zheng, J.-J. & Yu, X. N-cadherin-dependent neuron–
1099 neuron interaction is required for the maintenance of activity-induced dendrite growth. *Proc*.
1100 *Natl. Acad. Sci*. **107**, 9873–9878 (2010).
1101 54. Redies, C., Inuzuka, H. & Takeichi, M. Restricted expression of N- and R-cadherin on
1102 neurites of the developing chicken CNS. *J. Neurosci. Off. J. Soc. Neurosci*. **12**, 3525–3534
1103 (1992).
1104 55. Higashiyama, H. & Kuratani, S. On the maxillary nerve: The Maxillary Nerve in
1105 Vertebrates. *J. Morphol*. **275**, 17–38 (2014).
1106 56. Bronner-Fraser, M., Wolf, J. J. & Murray, B. A. Effects of antibodies against N-cadherin
1107 and N-CAM on the cranial neural crest and neural tube. *Dev. Biol*. **153**, 291–301 (1992).
1108 57. Shiau, C. E. & Bronner-Fraser, M. N-cadherin acts in concert with Slit1-Robo2 signaling
1109 in regulating aggregation of placode-derived cranial sensory neurons. *Development* **136**,
1110 4155–4164 (2009).
1111 58. Bill, B. R., Petzold, A. M., Clark, K. J., Schimmenti, L. A. & Ekker, S. C. A Primer for
1112 Morpholino Use in Zebrafish. *Zebrafish* **6**, 69–77 (2009).

1113 59. Stark, M. R., Sechrist, J., Bronner-Fraser, M. & Marcelle, C. Neural tube-ectoderm
1114 interactions are required for trigeminal placode formation. *Development* **124**, 4287–4295
1115 (1997).
1116 60. Lassiter, R. N. T., Stark, M. R., Zhao, T. & Zhou, C. J. Signaling mechanisms controlling
1117 cranial placode neurogenesis and delamination. *Dev. Biol.* **389**, 39–49 (2014).
1118 61. Wu, H.-H. *et al.* Glial precursors clear sensory neuron corpses during development via
1119 Jedi-1, an engulfment receptor. *Nat. Neurosci.* **12**, 1534–1541 (2009).
1120 62. Leonard, C. E., Quiros, J., Lefcort, F. & Taneyhill, L. A. Loss of Elp1 disrupts trigeminal
1121 ganglion neurodevelopment in a model of familial dysautonomia. *eLife* **11**, e71455 (2022).
1122 63. Basch, M. L., Bronner-Fraser, M. & García-Castro, M. I. Specification of the neural crest
1123 occurs during gastrulation and requires Pax7. *Nature* **441**, 218–222 (2006).
1124 64. Reis, S. A. *et al.* Striatal neurons expressing full-length mutant huntingtin exhibit
1125 decreased N-cadherin and altered neuritogenesis. *Hum. Mol. Genet.* **20**, 2344–2355 (2011).
1126 65. Shikanai, M. *et al.* Caveolin-1 Promotes Early Neuronal Maturation via Caveolae-
1127 Independent Trafficking of N-Cadherin and L1. *iScience* **7**, 53–67 (2018).
1128 66. Jontes, J. D. The Cadherin Superfamily in Neural Circuit Assembly. *Cold Spring Harb.*
1129 *Perspect. Biol.* **10**, a029306 (2018).
1130 67. Dady, A., Blavet, C. & Duband, J.-L. Timing and kinetics of E- to N-cadherin switch
1131 during neurulation in the avian embryo. *Dev. Dyn.* **241**, 1333–1349 (2012).

1132
1133
1134
1135
1136
1137